Broadened Low Anomalous Dispersion in Athermal Aluminum Nitride Hybrid Waveguides

Jianbin Ma , Ruiting Wang , Guangzhen Luo , Pengfei Ma, Pengfei Wang,
Yejin Zhang , and Jiaoqing Pan

Abstract—An aluminum nitride hybrid waveguide is proposed to reduce the challenges brought on by high temperature sensitivity of microresonator-based devices. The waveguide is temperature–insensitive (athermal) and has an effective thermo-optic coefficient value of $\pm 2 \times 10^{-6}$/K in the wavelength range of 1412 to 1800 nm. It exhibits anomalous dispersion of less than 96 ps/nm/km over octave in the range of 1540 to 3234 nm. The nonlinear coefficient of the aluminum nitride waveguide is enhanced by the strong nonlinearity of titanium oxide. Application of the athermal waveguide in the optical frequency comb is simulated to prove its superior thermo-optic performance.

Index Terms—Athermal waveguide, dispersion engineering, nonlinear optics, titanium dioxide.

I. INTRODUCTION

IN THE past decade, Si-based photonic devices attracted great attention due to the low propagation loss in them and mature manufacturing processes compatible with complementary metal-oxide-semiconductor (CMOS) technology. Due to the relatively large positive thermo-optic coefficient (TOC) of Si, photonic devices based on this material have high sensitivity to temperature variations [1], [2], which adversely affects their practical applications, especially in resonator-based devices for wavelength division, multiplexing or wideband nonlinear applications. To mitigate the temperature sensitivity of photonic devices, various methods were proposed for silicon [3], silicon nitride [4]–[6] and silica [7] platforms. However, athermal operation of aluminum nitride (AlN) devices, which is indispensable for their practical application, was not studied.

Due to the high quality of AlN films and strong nonlinear effects in them, many significant achievements were realized in nonlinear photonics using this material, which include wavelength conversion [8], formation of supercontinuum [9] and optical frequency combs (OFC) generation [10]. In nonlinear optics, nonlinear coefficient and dispersion are essential. Large values of the former enable to reduce turn-on and operation power. A flat and low dispersion, which can be achieved by dispersion engineering, is also strongly demanded [11]. Broadband low dispersion is usually desired to ensure phase matching condition over a wide spectral bandwidth [12]. Moreover, low dispersion enables to avoid signal distortion caused by pulse broadening and compression. Furthermore, thermal effects in the resonator are significantly enhanced in nonlinear applications that require accumulation of large power in the cavity. It causes unreliability in device performance [13], which is definitely a detrimental effect. This also calls a strong demand for athermal operation of microresonator-based nonlinear devices.

As compared to polymers, which are chemically unstable and susceptible to photodegradation [14], [15], titanium dioxide (TiO_2) is an ideal material with a negative TOC, 3-4 times higher than the one of AlN [4]. It is fully compatible with CMOS technology and has many desirable properties such as chemical and mechanical stability as well as compatibility with devices [16]. Titanium dioxide was used in various athermal devices on silicon and silicon nitride platforms [17], [18]. Moreover, TiO_2 has a relatively large nonlinear index, $n_2 = 2.3 \times 10^{-18}$ m^2/W, which is approximately 3 times larger than that of AlN [16]. Several nonlinear effects were recently demonstrated in TiO_2 waveguides, such as third harmonic generation, formation of supercontinuum, spectral broadening and four-wave mixing [16], [19]. However, high-quality low-loss waveguides based on TiO_2 are not easy to fabricate. Additional steps of the fabrication process, such as lift-off and bottom-up growth, are required [20], [21].

In this paper, we propose and numerically study for the first time an AlN/TiO_2 hybrid waveguide structure with three properties improved as compared to traditional waveguides. TiO_2 is used as a cladding material to coat the whole AlN waveguide structure with the purpose of engineering its thermo-optic coefficient, broadening low anomalous dispersion and enhancing nonlinearity. Since TiO_2 has significantly large TOC value, a thin layer of this material is sufficient to compensate for the positive TOC of AlN without the need for a lift-off or etching process. The effective nonlinear coefficient of the obtained hybrid waveguide increases due to the large value of the nonlinear coefficient of TiO_2.

The authors are with the Key Laboratory of Semiconductor Materials Science, Institute of Semiconductors, Chinese Academy of Sciences, Beijing 100083, China and also with the University of Chinese Academy of Sciences, Beijing 100049, China (e-mail: majianbin@semi.ac.cn; rtwang@semi.ac.cn; gzhenluo@semi.ac.cn; pfma@semi.ac.cn; pfwang15@semi.ac.cn; yjzhang@semi.ac.cn; jqpan@semi.ac.cn).
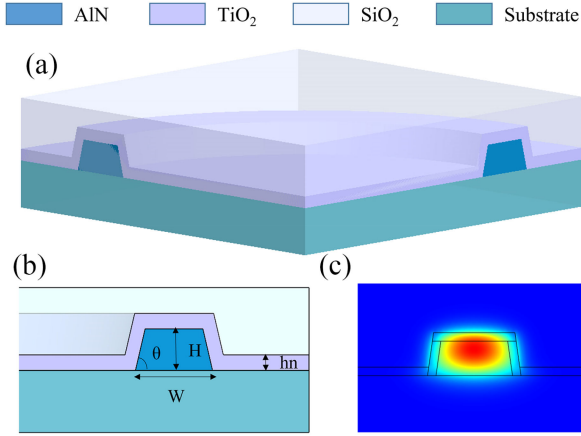
Fig. 1. Structure of hybrid waveguide. Its main parameters are *W, H, hn* and *θ*. (b) Smooth optical mode field profile of fundamental quasi-TE mode is due to the similar refractive indices of aluminum nitride and titanium oxide.

TABLE I
TOC AND N_2 OF HYBRID WAVEGUIDE MATERIALS

Material	AlN	TiO₂	SiO₂	Sapphire
TOC $(10^{-5}/°C)$	2.7 [25]	-10 [5]	1.0 [5]	0.125 [26, 27]
n_2 $(10^{-19}m^2·W^{-1})$	3.5 [28]	23 [16]	0.276 [29]	0.28 [30]

by the following expression:

$$\frac{dn_{eff}}{dT} = \sum_{i}^{N} \Gamma_i \frac{dn_i}{dT} \tag{2}$$

Here, the effective TOC of the waveguide is given as the first derivative of the effective refractive index of the waveguide with respect to temperature. We can write it as follows:

$$TOC_{eff} \approx \Gamma_{AlN}TOC_{AlN} + \Gamma_{SiO2}TOC_{SiO2}$$
$$+ \Gamma_{TiO2}TOC_{TiO2} \tag{3}$$

When the athermalized waveguide considered here is used together with microring resonators with different radii, the effective TOC of the latter remains almost unchanged. We can directly calculate the relationship between TDWS (temperature dependent wavelength shift) and wavelength using the relationship between the former and TOC [3]. Since TiO₂ is used only as the temperature compensation material for AlN waveguide, due to its large thermo-optical coefficient a thin TiO₂ film can compensate for the thermo-optic effect of thick AlN film. By simulating and optimizing the waveguide structure, its structural dimensions that meet the required demands are obtained. The TOC and n_2 values of the materials we used are shown in Table I.

II. PRINCIPLE AND DESIGN

In view of the excellent properties of both AlN and TiO₂ materials, a simple waveguide structure is sufficient to meet all the demands, which include small thermo-optic coefficient, low anomalous dispersion in the wide band and large nonlinear coefficient. The structure of the hybrid waveguide considered in this work is shown in Fig. 1. AlN core layer of the waveguide has the thickness H, width W and sidewall inclination angle *θ*, respectively. hn is the thickness of the TiO₂ compensation layer. Such design of the waveguide structure enables to obtain high-quality TiO₂ films without use of complicated processing techniques. Moreover, the hybrid waveguide can retain the original excellent optical properties of single-crystalline aluminum nitride [22], unlike slot waveguides that require multiple growth processes resulting in extra losses [23].

The main optical parameters in the simulations were the effective refractive index and mode field distribution in the hybrid waveguide. As shown in Fig. 1, the athermal hybrid waveguide mainly consists of four parts, namely the AlN central layer, the TiO₂ layer, the substrate, and the Si oxide cover layer.

We used the finite element method (FEM) implemented in the COMSOL Multiphysics software to calculate the effective refractive index of the proposed waveguide structure. A perfect matched layer (PML) boundary condition was applied to the outermost silica layer to absorb the power leaking outwards. The effective refractive index of the waveguide can be expressed as follows [24]:

$$n_{eff} = \sum_{i}^{N} \Gamma_i n_i \tag{1}$$

where n_i are the refractive indices of each material composing the waveguide, and Γ_i are the field limiting factors of the substrate, core, compensation layer and cladding layer, respectively.

In general, the Γ_i values remain fairly invariant within a moderate range of temperature variation. Therefore, the thermo-optic property of guided mode is dominated by them, which is given

III. RESULTS AND DISCUSSION

Taking into account the waveguide structure proposed in this work, three main parameters of the waveguide, namely H, W and hn were simulated and optimized. First, we simulated the effective TOC values at the values of structural parameters in a certain range. After that, the dispersion curve was calculated using the obtained effective TOC values. Finally, the nonlinear coefficients of the waveguide were found. The optimal waveguide structure was selected by comparing the performance of waveguides with different parameters.

A. Thermo-Optic Property

In order to realize the temperature compensation effect by TiO₂, its thickness should change with the change of the AlN structure. We calculated the effective TOC values for a series of waveguide structures with varying parameters. In particular, the structures with W changing from 2.0 to 3.5 μm, H changing from 0.7 to 1.1 μm and hn changing from 0.15 to 0.35 μm were considered. The calculation results mainly showing the relationship between the effective TOC value at 1550 nm and the values of three dimensions indicated above are presented.
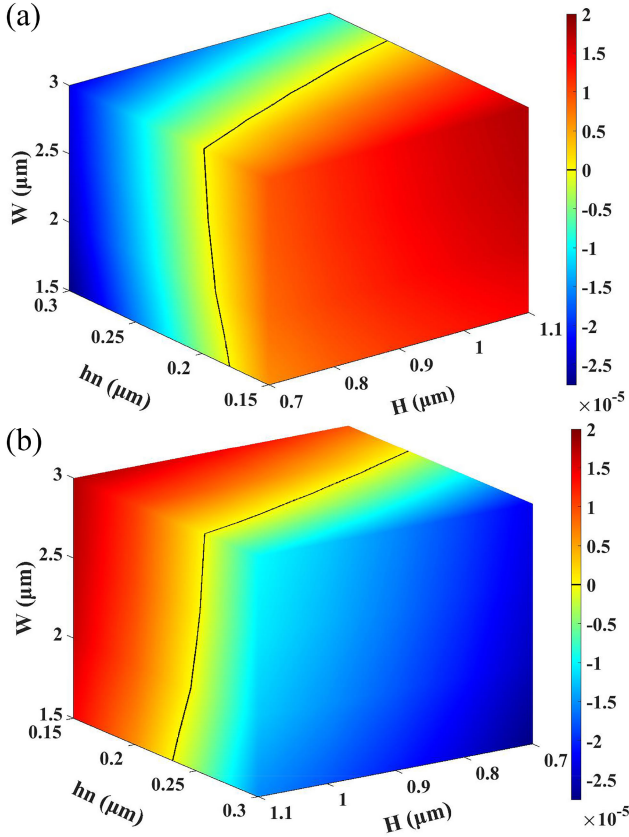
Fig. 2.   Variation of effective TOC with AlN width *W* and thickness *H* and TiO$_2$ thickness *hn*.

Fig. 3.   Variation of dispersion with (a) width and (b) height of AlN, and (c) TiO$_2$ layer thickness.

The black curves in Fig. 2 correspond to the effective TOC values equal to 0 at 1550 nm. The color bars on the right show the effective TOC scales. Three structural parameters have an impact on the effective TOC value of the hybrid waveguide. Among them, the thickness of TiO$_2$ is an important characteristic, which significantly influences on the effective TOC. It can be clearly seen from Fig. 2 that the increase of this thickness leads to a gradual change of the effective TOC from positive to negative values. Furthermore, the size of the core waveguide has also a strong effect on the effective TOC value. With the increase of waveguide size, this value gradually becomes positive, indicating that thicker titanium oxide is required to balance the effect of temperature variation. Equation (3) demonstrates that more optical mode field is confined in the core layer of large-scale waveguide. When the thickness of TiO$_2$ increases, more optical energy, becomes distributed in it and less energy in AlN. This leads to more uniform distribution of optical field and facilitates the compensation of temperature effect.

B. Dispersion and Nonlinear Coefficients

Dispersion plays an important role in nonlinear applications. Dispersion engineering is an important technique to control the dispersion of waveguides to meet different requirements: normal dispersion or anomalous one. In this section, we calculate the di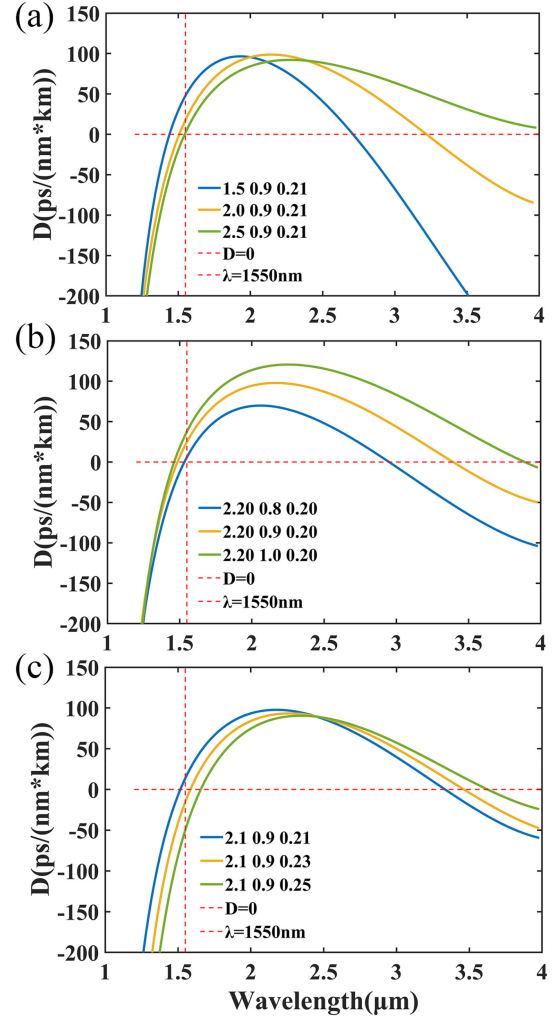spersion for waveguide structures with the parameters obtained in Section III-A. The group velocity dispersion (GVD) parameter D is used to characterize the second-order dispersion. This parameter is calculated by the following formula:

$$D = \frac{\lambda}{c} \frac{d^2 n_{eff}}{d\lambda^2} \qquad (4)$$

where n_{eff} is the effective refractive index of the waveguide, λ is the wavelength of light, and c is the speed of light in vacuum, respectively. $D > 0$ corresponds to normal dispersion and $D < 0$ to anomalous dispersion, respectively.

We carried out numerical simulations to determine the values of GVD parameter for different waveguide geometries. Obtained results are shown in Fig. 3. The dependences presented in Fig. 3(a) demonstrate that increase of the width of the core waveguide leads to the shift of the dispersion curve to longer wavelengths. At this, longer-wavelength zero dispersion point rapidly shifts in the same direction and the dispersion curve flattens. Fig. 3(b) shows that the value of dispersion increases and the dispersion curve shifts upward at the increase of the core waveguide height. As can be further seen from Fig. 3(c), increase of the thickness of TiO$_2$ compensation layer induces the shift of
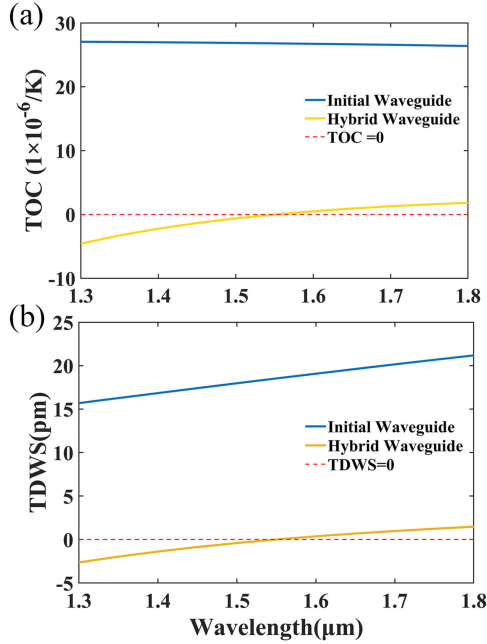
Fig. 4. TOC and TDWS versus wavelength for AlN waveguide without and with TiO_2 compensation layer.
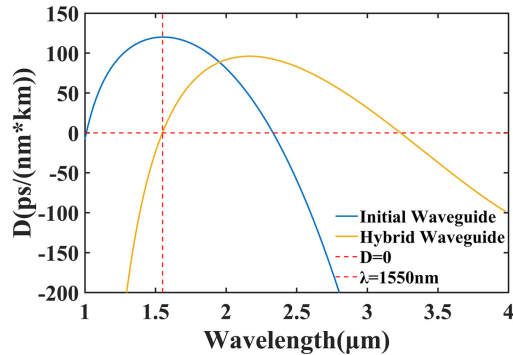

Fig. 5. Dispersion curves for AlN waveguide without and with TiO_2 compensation layer.

GVD towards negative (normal) values. However, according to the results of the calculations of thermo-optic performance, the thickness of TiO_2 layer should be increased accordingly with the increase of the size of the core layer waveguide. Therefore, the structure of the waveguide should be properly optimized.

The optimum thermo-optical property, low anomalous dispersion value and extremely small TOC values at 1550 nm of hybrid waveguides are obtained at the thickness $hn = 0.222$ μm of TiO_2 layer deposited on the initial waveguide with $W = 2.0$ μm, $H = 0.9$ μm, and $\theta = 80°$. As shown in Fig. 4, the hybrid waveguide has a near-zero broadband effective TOC value of $\pm 2 \times 10^{-6}$/K over the bandwidth from 1412 to 1800 nm. The TDWS of the athermal microring resonator can be kept within ± 1 pm/K in the wavelength range of 1436 to 1705 nm. Besides, this hybrid waveguide has superior dispersion performance as compared to the initial AlN waveguide, as can be seen in Fig. 5. As shown in this figure, it has flat low anomalous dispersion over an octave bandwidth and anomalous
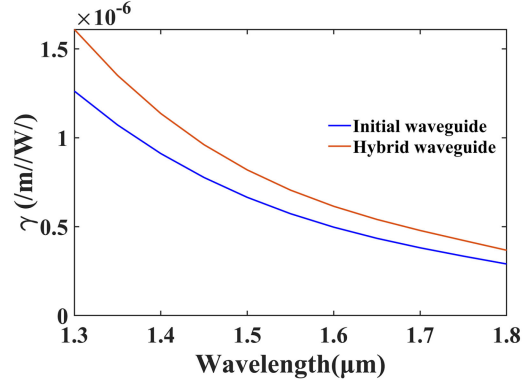

Fig. 6. γ versus wavelength for AlN waveguide without and with TiO_2 compensation layer.

dispersion with the maximum of 96 ps/nm/km in the wavelength range of 1540 to 3234 nm. Although the hybrid waveguide consists of different materials, namely TiO_2 and AlN, they have a moderate difference in refractive indices. Therefore, the profile of electric field mode changes smoothly in the waveguide core region with no abrupt changes like the ones observed in slot waveguides, as shown in Fig. 1(b).

The origin of the nonlinear refractive index of optical materials is the third-order susceptibility term (χ^3) of induced polarization as described in [31]. The effect of this characteristic on optical waveguides is usually described by the nonlinear parameter γ, which is expressed as follows [32]:

$$\gamma = \frac{2\pi \cdot n_2}{\lambda \cdot A_{eff}} \qquad (5)$$

Here, λ is the wavelength of light and A_{eff} is the effective mode area, respectively. Based on [33], we calculated the variations of nonlinear coefficients for the initial and the hybrid waveguide in the wavelength range of 1300 to 1800 nm. Respective results are shown in Fig. 6. As can be seen from this figure, the nonlinear coefficient of the hybrid waveguide is significantly enhanced as compared to the one for the initial waveguide.

In practice, fabrication errors are inevitable. They have a significant impact on the effective TOC value and dispersion. The error ranges are different depending on the fabrication steps. For evaluation of the fabrication error tolerances of the multilayer hybrid waveguide, the effects of structural parameters on the athermal and dispersion properties were studied. This study was performed by changing each of these parameters around the optimum values, while keeping the rest ones constant. We varied the values of the structural parameters W, H, hn and θ. The variation ranges were as follows: W was varied from 1.9 to 2.1 μm at the step of 0.1 μm; H was varied from 0.85 to 0.95 μm at the step of 0.05 μm; hn was varied from 0.212 to 0.232 μm at the step of 0.01 μm; and θ was varied from 75° to 85° at the step of 5°.

The results of this study are shown in Figs. 7 and 8. It can be seen from these figures that when the width of AlN increased from 1.9 to 2.1 μm, the effective TOC values changed from -3.6×10^{-7}/K to 3.5×10^{-7}/K at 1550 nm and the anomalous dispersion wavelength range changed from 1530–3115 to
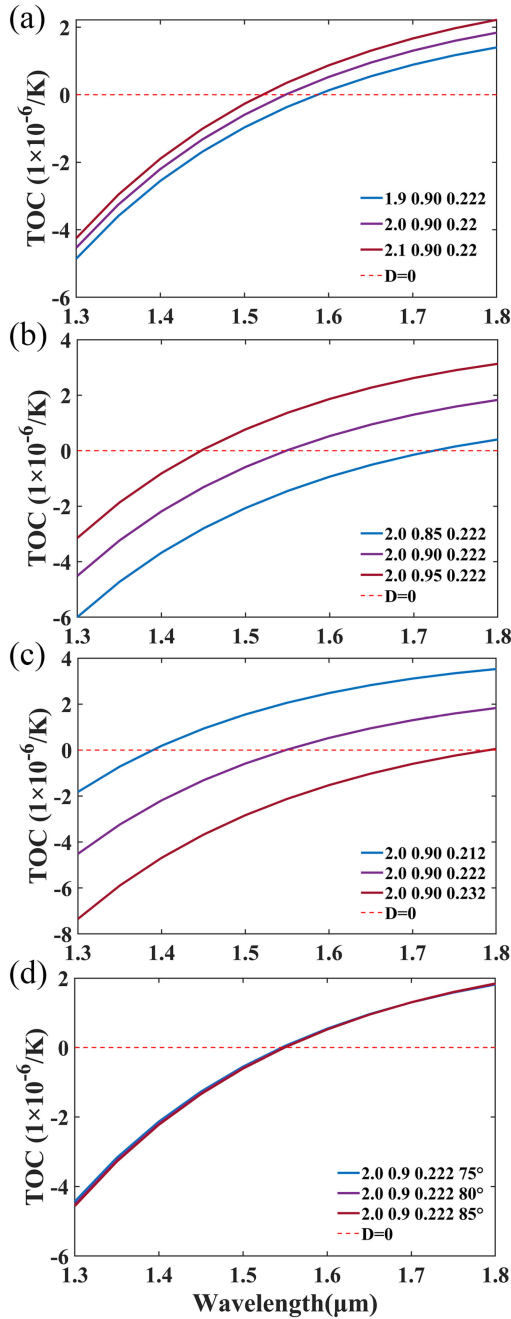
Fig. 7. Shifts of effective TOC curves with (a) width and (b) height of AlN, (c) TiO$_2$ layer thickness and (d) sidewall inclination angle.
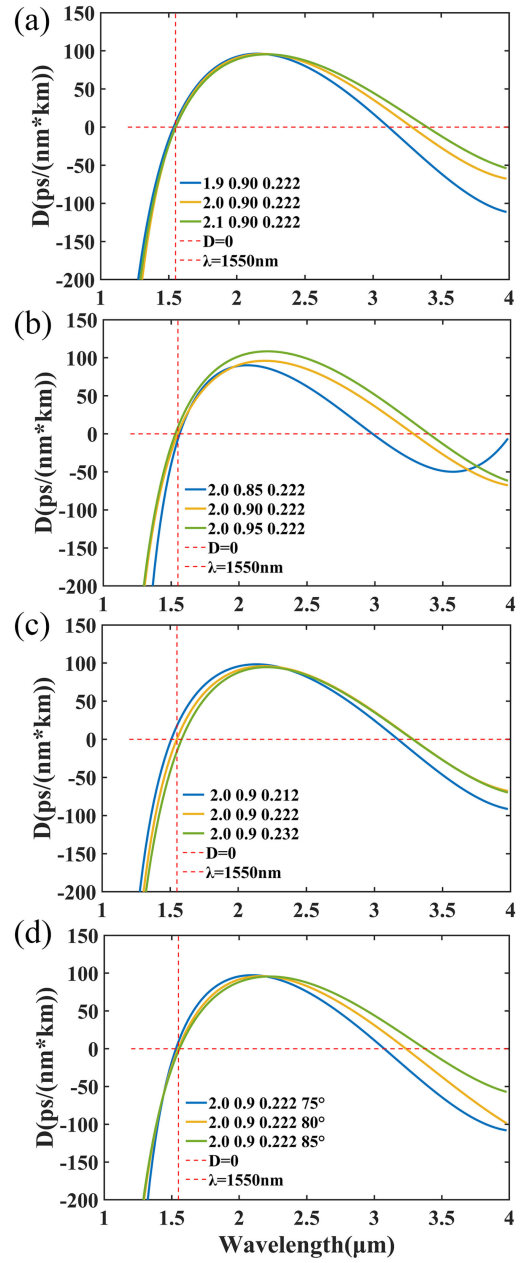

Fig. 8. Change of dispersion curves with (a) width and (b) height of AlN, (c) TiO$_2$ layer thickness and (d) sidewall inclination angle.

1551–3397 nm. When the height of AlN increased from 0.85 to 0.95 μm, the effective TOC values increased from -1.45×10^{-6}/K to 1.368×10^{-6}/K at 1550 nm and the anomalous dispersion wavelength range changed from 1531-2984 to 1560-3398 nm. At the variation of the thickness of the TiO$_2$ compensation layer from 0.212 to 0.232 μm, the effective TOC values increased from -2.123×10^{-6}/K to 2.06×10^{-6}/K at 1550 nm and the anomalous dispersion wavelength range changed from 1531–2984 to 1560–3398 nm. As for the sidewall inclination θ, the change of the effective TOC value was extremely small, within $\pm 2.06 \times 10^{-8}$/K, varying θ from 75° to 85°, and the

anomalous dispersion wavelength range changed from 1531–3074 to 1557–3376 nm at this. From these results, a conclusion about different effects of the considered four parameters on the effective TOC value and dispersion can be drawn. At this, the width and the thickness of aluminum nitride core layer are the main influencing factors. The thickness of titanium oxide as the temperature compensation layer has a great influence on the value of TOC, but its effect on the dispersion is much weaker. The sidewall inclination angle has a great influence on the dispersion but little effect on the TOC value.

In device technologies, single-crystalline AlN films are grown on sapphire substrates by metal organic chemical vapor deposition (MOCVD) [34], which enables to control the error
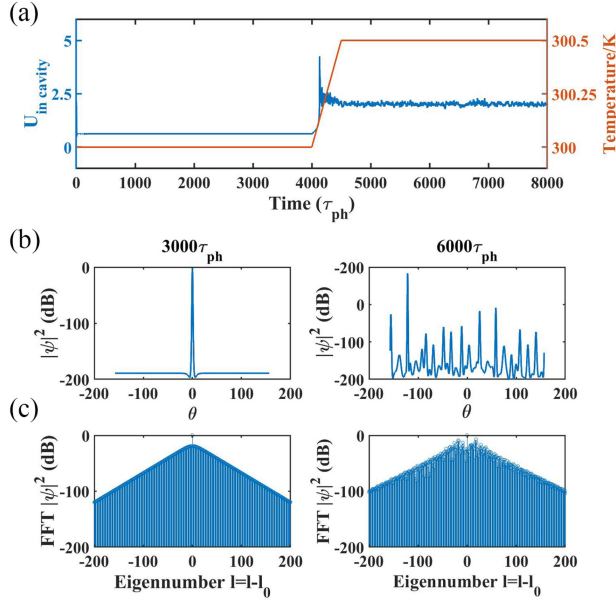
Fig. 9. (a) The temperature (red curve) and the average round trip energy (blue) in the initial waveguide cavity. The time domain and the corresponding frequency domain at $3000\tau_{\rm ph}$ (b) and $6000\tau_{\rm ph}$ (c).
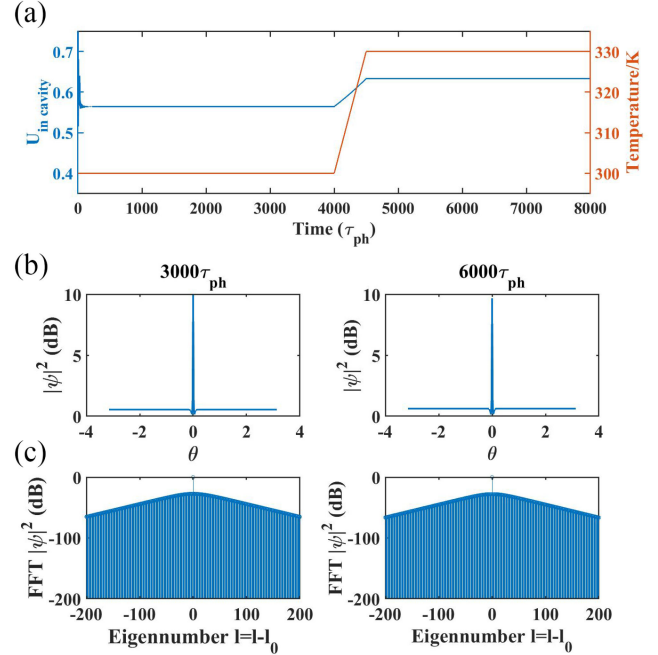

Fig. 10. (a) The temperature (red curve) and the average round trip energy (blue) in the hybrid waveguide cavity. The time domain and the corresponding frequency domain at $3000\tau_{\rm ph}$ (b) and $6000\tau_{\rm ph}$ (c).

range of the layer thickness within tens of nm. Atomic layer deposition (ALD) of TiO_2 [35] provides a better control of the thickness error in the range of a few nm. The sidewall inclination angle θ is closely related to the etching conditions of AlN and is a definite value when these conditions are fixed. Therefore, we present the guidance for effective tailoring TOC and dispersion of the proposed waveguides to achieve the desired waveguide properties.

C. Optical Frequency Comb Application

To demonstrate the influence of temperature on OFC generation in different waveguides, we simulated the generation of a comb using the Lugiato–Lefever equation [36], [37]:

$$\frac{\partial \psi}{\partial \tau} = -(1 + i\alpha)\psi + i|\psi|^2\psi - i\frac{\beta}{2}\frac{\partial^2 \psi}{\partial \theta^2} + F \quad (6)$$

In these simulations, the quality factor was set to be 10^6 and the values of dispersions around 1550 nm were 120.078 and 0.6596 ps/nm/km for the initial and the athermal hybrid waveguide, respectively. When the radii of two microrings are both equal to 100 μm, the values of TDWS around 1550 nm for microring resonators with the strip and the athermal hybrid waveguide are 18.529 and 0.00383 pm/K, respectively. We simulated the OFC generation in different waveguides at slow temperature changes at the pump power $F^2 = 6.5$. Figs. 9 and 10 show the results obtained at the application of the initial and the hybrid waveguide in the microcavity, respectively.

As can be seen from Fig. 9, raise of the temperature from 300 to 300.2 K for the microcavity with the initial waveguide, induced apparent change of the average round trip energy in the cavity. The state of OFC changed from the soliton (at $3000 \tau_{\rm ph}$, where $\tau_{\rm ph}$ is the photon lifetime) to the chaotic one (at $6000 \tau_{\rm ph}$)

in the time-domain, as shown in Fig. 9(b), and the envelope of the comb lines became irregular in the frequency domain, as shown in Fig. 9(c). Respective results for the hybrid waveguide obtained under the same initial detuning conditions are shown in Fig. 10. When the temperature of the hybrid waveguide was raised from 300 to 330 K, the average round trip energy change in the cavity was small. The OFC state remained the soliton one (at $3000 \tau_{\rm ph}$ and $6000 \tau_{\rm ph}$). This means that the microcavity based on the hybrid waveguide has a good thermal stability as compared to that of the initial AlN based microcavity.

IV. CONCLUSION

In this work, a hybrid waveguide with a near-zero broadband effective TOC values of $\pm 2 \times 10^{-6}$/K over the bandwidth of 1412 to 1800 nm is proposed. This waveguide shows a low anomalous dispersion over an octave and an anomalous dispersion of less than 96 ps/nm/km in the wavelength range of 1540 to 3234 nm. The nonlinear coefficient of the hybrid waveguide is enhanced as compared to the one of the initial AlN waveguide. In addition, we numerically simulated the effect of temperature change on the generation of OFC by comparing a traditional strip waveguide with the hybrid one. We proved that the athermal hybrid waveguide has a pretty good thermal stability. Obtained results are significant for AlN waveguides for athermalized device and nonlinear applications.

ACKNOWLEDGMENT

References

[1] B. Guha, J. Cardenas, and M. Lipson, "Athermal silicon microring resonators with titanium oxide cladding," *Opt. Exp.*, vol. 21, no. 22, pp. 26557–26563, Nov. 2013, doi: 10.1364/OE.21.026557.

[2] V. S. Afshar, T. M. Monro, and C. M. de Sterke, "Understanding the contribution of mode area and slow light to the effective Kerr nonlinearity of waveguides," *Opt. Exp.*, vol. 21, no. 15, pp. 18558–18571, Jul. 2013, doi: 10.1364/oe.21.018558.

[3] V. Raghunathan, W. N. Ye, J. Hu, T. Izuhara, J. Michel, and L. Kimerling, "Athermal operation of silicon waveguides: Spectral, second order and footprint dependencies," *Opt. Exp.*, vol. 18, no. 17, pp. 17631–17639, Aug. 2010, doi: 10.1364/OE.18.017631.

[4] F. Qiu, A. M. Spring, F. Yu, and S. Yokoyama, "Complementary metal-oxide-semiconductor compatible athermal silicon nitride/titanium dioxide hybrid micro-ring resonators," *Appl. Phys. Lett.*, vol. 102, no. 5, Feb. 2013, Art. no. 051106, doi: 10.1063/1.4790440.

[5] L. Q. He *et al.*, "Broadband athermal waveguides and resonators for datacom and telecom applications," *Photon. Res.*, vol. 6, no. 11, pp. 987–990, Nov. 2018, doi: 10.1364/Prj.6.000987.

[6] T. D. Bucio, A. Z. Khokhar, G. Z. Mashanovich, and F. Y. Gardes, "Athermal silicon nitride angled MMI wavelength division (de)multiplexers for the near-infrared," *Opt. Exp.*, vol. 25, no. 22, pp. 27310–27320, Oct. 2017, doi: 10.1364/OE.25.027310.

[7] N. Kobayashi, N. Zaizen, and Y. Kokubun, "Athermal and polarization-independent microring resonator filter using stress control," *Japanese J. Appl. Phys. Part 1-Regular Papers Brief Commun. Rev. Papers*, vol. 46, no. 8b, pp. 5465–5469, Aug. 2007, doi: 10.1143/Jjap.46.5465.

[8] X. Liu, A. W. Bruch, and H. X. Tang, "AlN nonlinear optics and integrated photonics," *Semiconductors Semimetals*, vol. 107, pp. 223–281, 2021.

[9] J. Lu *et al.*, "Ultraviolet to mid-infrared supercontinuum generation in single-crystalline aluminum nitride waveguides," *Opt. Lett.*, vol. 45, no. 16, pp. 4499–4502, Aug. 2020, doi: 10.1364/OL.398257.

[10] Z. Gong *et al.*, "High-fidelity cavity soliton generation in crystalline AlN micro-ring resonators," *Opt. Lett.*, vol. 43, no. 18, pp. 4366–4369, Sep. 2018, doi: 10.1364/OL.43.004366.

[11] Y. Okawachi *et al.*, "Bandwidth shaping of microresonator-based frequency combs via dispersion engineering," *Opt. Lett.*, vol. 39, no. 12, pp. 3535–3538, Jun. 2014, doi: 10.1364/OL.39.003535.

[12] M. H. P. Pfeiffer *et al.*, "Octave-spanning dissipative Kerr soliton frequency combs in Si$_3$N$_4$ microresonators," *Optica,* vol. 4, no. 7, pp. 684–691, Jul. 2017, doi: 10.1364/Optica.4.000684.

[13] C. Bao, Y. Xuan, J. A. Jaramillo-Villegas, D. E. Leaird, M. Qi, and A. M. Weiner, "Direct soliton generation in microresonators," *Opt. Lett.*, vol. 42, no. 13, pp. 2519–2522, Jul. 2017, doi: 10.1364/OL.42.002519.

[14] C. Decker and K. Zahouily, "Photodegradation and photooxidation of thermoset and UV-cured acrylate polymers," *Polym. Degradation Stability*, vol. 64, no. 2, pp. 293–304, 1999, doi: 10.1016/S0141-3910(98)00205-5.

[15] A. M. Spring, F. Qiu, K. Yamamoto, S. Yokoyama, and Y. Feng, "0.018 pm/°C athermal silicon nitride ring resonator by polymer cladding," in *Proc. Conf. Lasers Electro-Opt. Pacific Rim*, 2013, pp. 1–2.

[16] X. W. Guan, H. Hu, L. K. Oxenlowe, and L. H. Frandsen, "Compact titanium dioxide waveguides with high nonlinearity at telecommunication wavelengths," *Opt. Exp.*, vol. 26, no. 2, pp. 1055–1063, Jan. 2018, doi: 10.1364/Oe.26.001055.

[17] F. Qiu, A. M. Spring, F. Yu, and S. Yokoyama, "Complementary metal–oxide–semiconductor compatible athermal silicon nitride/titanium dioxide hybrid micro-ring resonators," *Appl. Phys. Lett.*, vol. 102, no. 5, 2013, Art. no. 51106.

[18] B. Guha, B. B. Kyotoku, and M. Lipson, "CMOS-compatible athermal silicon microring resonators," *Opt. Exp.*, vol. 18, no. 4, pp. 3487–3493, Feb. 2010, doi: 10.1364/OE.18.003487.

[19] M. Fu *et al.*, "High-Q titanium dioxide micro-ring resonators for integrated nonlinear photonics," *Opt. Exp.*, vol. 28, no. 26, pp. 39084–39092, Dec. 2020, doi: 10.1364/OE.404821.

[20] G. Li, M. Fu, Y. Zheng, and X. Guan, "TiO$_2$ microring resonators with high Q and compact footprint fabricated by a bottom-up method," *Opt. Lett.*, vol. 45, no. 18, pp. 5012–5015, Sep. 2020, doi: 10.1364/OL.400644.

[21] C. C. Evans, C. Y. Liu, and J. Suntivich, "Low-loss titanium dioxide waveguides and resonators using a dielectric lift-off fabrication process," *Opt. Exp.*, vol. 23, no. 9, pp. 11160–11169, May 2015, doi: 10.1364/Oe.23.011160.

[22] X. Liu *et al.*, "Aluminum nitride-on-sapphire platform for integrated high-Q microresonators," *Opt. Exp.*, vol. 25, no. 2, pp. 587–594, Jan. 2017, doi: 10.1364/OE.25.000587.

[23] J. Y. Li, K. Xu, and J. B. Du, "Ultrabroadband and flattened dispersion in aluminum nitride slot waveguides," *IEEE Photon. J.*, vol. 9, no. 4, Aug. 2017, Art. no. 2700408, doi: 10.1109/Jphot.2017.2716956.

[24] T. Lipka, L. Moldenhauer, J. Mueller, and H. K. Trieu, "Athermal and wavelength-trimmable photonic filters based on TiO$_2$-cladded amorphous-SOI," *Opt. Exp.*, vol. 23, no. 15, pp. 20075–20088, Jul. 2015, doi: 10.1364/Oe.23.020075.

[25] N. Watanabe, T. Kimoto, and J. Suda, "The temperature dependence of the refractive indices of GaN and AlN from room temperature up to 515 °C," *J. Appl. Phys.*, vol. 104, no. 10, Nov. 2008, Art. no. L1998, doi: 10.1063/1.3021148.

[26] M. E. Thomas, S. K. Andersson, R. M. Sova, and R. I. Joseph, "Frequency and temperature dependence of the refractive index of sapphire," *Infrared Phys. Technol.,* vol. 39, no. 4, pp. 235–249, Jun. 1998, doi: 10.1016/S1350-4495(98)00010-3.

[27] P. Dragic, T. Hawkins, P. Foy, S. Morris, and J. Ballato, "Sapphire-derived all-glass optical fibres," *Nature Photon.*, vol. 6, no. 9, pp. 627–633, Sep. 2012, doi: 10.1038/Nphoton.2012.182.

[28] X. Liu *et al.*, "Integrated High-Q crystalline AlN microresonators for broadband Kerr and Raman frequency combs," *ACS Photon.,* vol. 5, no. 5, pp. 1943–1950, 2018, doi: 10.1021/acsphotonics.7b01254.

[29] T. Kato, Y. Suetsugu, and M. Nishimura, "Estimation of nonlinear refractive index in various silica-based glasses for optical fibers," *Opt. Lett.*, vol. 20, no. 22, pp. 2279–2281, Nov. 1995, doi: 10.1364/ol.20.002279.

[30] A. Major, F. Yoshino, I. Nikolakakos, J. S. Aitchison, and P. W. Smith, "Dispersion of the nonlinear refractive index in sapphire," *Opt. Lett.*, vol. 29, no. 6, pp. 602–604, Mar. 2004, doi: 10.1364/ol.29.000602.

[31] G. Agrawal, *Nonlinear Fiber Optics*. Amsterdam, Netherlands/Cambridge, MA, USA: Elsevier/Academic. 2013, pp. 27–56.

[32] V. S. Afshar, T. Monro, and C. M. de Sterke, "Understanding the contribution of mode area and slow light to the effective Kerr nonlinearity of waveguides," *Opt. Exp.*, vol. 21, no. 15, pp. 18558–18571, Jul. 2013, doi: 10.1364/oe.21.018558.

[33] Y. Yang *et al.*, "Invited article: Enhanced four-wave mixing in waveguides integrated with graphene oxide," *APL Photon.*, vol. 3, no. 12, 2018, Art. no. 120803.

[34] J. Liu *et al.*, "Photolithography allows high-Q AlN microresonators for near octave-spanning frequency comb and harmonic generation," *Opt. Exp.,* vol. 28, no. 13, pp. 19270–19280, Jun. 2020, doi: 10.1364/OE.395013.

[35] J.-P. Niemelä, G. Marin, and M. Karppinen, "Titanium dioxide thin films by atomic layer deposition: A review," *Semicond. Sci. Technol.*, vol. 32, no. 9, 2017, Art. no. 093005.

[36] S. Coen and M. Erkintalo, "Universal scaling laws of Kerr frequency combs," *Opt. Lett.*, vol. 38, no. 11, pp. 1790–1792, Jun. 2013, doi: 10.1364/OL.38.001790.

[37] Y. K. Chembo and C. R. Menyuk, "Spatiotemporal Lugiato-Lefever formalism for Kerr-comb generation in whispering-gallery-mode resonators," *Phys. Rev. A*, vol. 87, no. 5, May 2013, Art. no. 053852, doi: 10.1103/PhysRevA.87.053852.